Available online at www.sciencedirect.com
ScienceDirect
Trans. Nonferrous Met. Soc. China 20(2010) 1968−1973
Transactions of Nonferrous Metals Society of China
www.tnmsc.cn

Void damage evolution of LF6 aluminum alloy welded joints under external load and thermal cycling conditions

MI Guo-fa(米国发)[1], ZHAO Da-wei(赵大为)[1], DONG Cui-fen(董翠粉)[1],
NIU Ji-tai(牛济泰)[1, 2], JIN Cheng(金 成)[3]

1.School of Materials Science and Engineering, Henan Polytechnic University, Jiaozuo 454003, China;
2. School of Materials Science and Engineering, Harbin Institute of Technology, Harbin 150001, China;
3. School of Materials Science and Engineering, Dalian Jiaotong University, Dalian 116028, China

Received 16 October 2009; accepted 22 March 2010

Abstract: Based on the simulated aerospace thermal cycling tests, the effect of thermal cycle on the void damage evolution mechanism of LF6 aluminum alloy welded joint was investigated. The results show that micro-voids form around the second phase particles under the thermal cycling tests. The thermal stress coupled with external stress leads to dislocations pile-up around the particles, and when the dislocation density reaches a certain degree, the stress concentration will exceed the bonding strength at the interface between particles and matrix, resulting in the formation of micro-cracks. The numerical simulation is successfully implemented with the finite element to describe the void damage evolution of the welded joint under thermal cycling conditions.
Key words: aluminum alloy; welded joint; thermal stress; numerical simulation; micro-void

1 Introduction

During the space vehicles moving in low-earth orbit, some shell constructions are subjected to the space cyclic thermal load as well as the working loads. The extreme temperature range of the thermal cycling encountered is 93−393 K[1−3], Which will cause the performances deterioration and material microstructure damage[4]. Much work had been done on the damage of composites induced by thermal cycling[5−6], but little attention has been given to investigate the thermal cycling induced damage of metals or its welded joints.

Aluminum alloy is an important lightweight construction material in aerospace industries[7]. Aluminum alloy welded structures have been widely used to construct the shell module of space vehicles. But the welded joint often becomes the weakest part of the whole welded construction in some conditions[8−11]. In order to evaluate the long-life reliability and guarantee the safety of the welded structure under services, it is essential to determine its void damage mechanisms. In this work, the void nucleation and evolution in a LF6 aluminum alloy butt-welded joint were studied under simulated space thermal cycling conditions.

2 Experimental

2.1 Materials and welding condition

A typical composition of the parent aluminum alloy LF6 sheet used in this study is presented in Table 1. The sheets with 5 mm in thickness were butt-welded by variable polarity plasma arc welding (VPPAW) using the same filler wire material. Table 2 lists the VPPAW conditions. Welded joint specimens were cut across the butt-join welded sheets, as shown in Fig.1.

Table 1 Chemical composition of test material (mass fraction, %)

Mg	Mn	Ti	Fe	Si
5.8−6.8	0.5−0.8	0.02−0.1	≤0.4	≤0.4
Zn	Al	Cu	Other	
≤0.2	Bal.	≤0.1	≤0.1	

Foundation item: Project(90205035) supported by the National Natural Science Foundation of China
Corresponding author: ZHAO Da-wei; Tel: +86-391-3987503; E-mail: peten@hpu.edu.cn
DOI: 10.1016/S1003-6326(09)60403-9

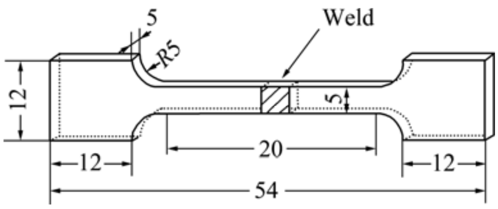

Fig.1 Dimension of welded joint specimens (mm)

X-ray non-destructive detections were carried out on these welded specimens. The specimens with any detectable defect were eliminated to ensure the results consistency in the following tests.

2.2 Thermal cycling test

Thermal cycling tests were conducted using a homemade machine. Several welded joint specimens were put into the thermal isolation cavity of the machine. During the test, an external tensile load of 100 MPa was applied to the specimens. The specimens were heated using a resistant heater and cooled by spraying liquid nitrogen into the test cavity. In order to simulate the low-earth orbit thermal cycle, the cycle temperature range is 173−373 K and the cyclic period is 90 min. A thermocouple was fixed on the specimen surface in order to realize real-time temperature monitor. All test parameters were preprogrammed and input into the supervisory control computer, and a total of 100 cycles were recorded for each test. A schematic diagram of thermal cycling of one cycle is shown in Fig.2.

To study the change of microstructures and damage evolution, especially the nucleation of the micro-void, different sections of the welded joint specimens were sampled before and after the thermal cycling test. The microstructures of these samples were observed using an optical microscope for the mesoscale. The fracture surfaces of the tensile specimens were observed by SEM. Typical chemical compositions were determined quantitatively using EDS. Dislocation configuration characteristics were appraised using TEM. The numerical simulation was implemented to describe the void damage evolution of the welded joint under thermal cycling conditions.

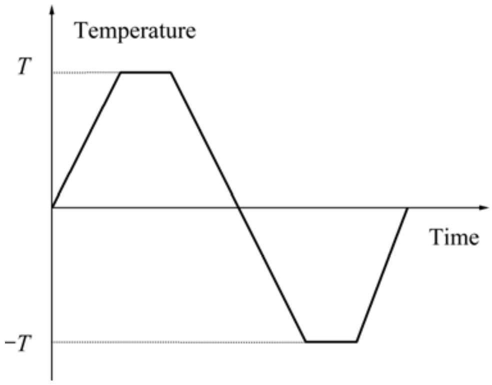

Fig.2 Schematic diagram of thermal cycling

3 Results and discussion

The original microstructures of different zones of the welded joint are shown in Fig.3. The second phase

Table 2 Parameters of welding process

Filler wire material	Argon flow rate/ $(L\cdot min^{-1})$	Current of DCNE/ A	Current of DCPE/ A	Time of DCNE/ ms	Time of DCPE/ ms	Welding speed/ $(m\cdot min^{-1})$
LF6	2.0	130	160	21	4	0.18

DCNE: direct current negative electrode; DCPE: direct current positive electrode

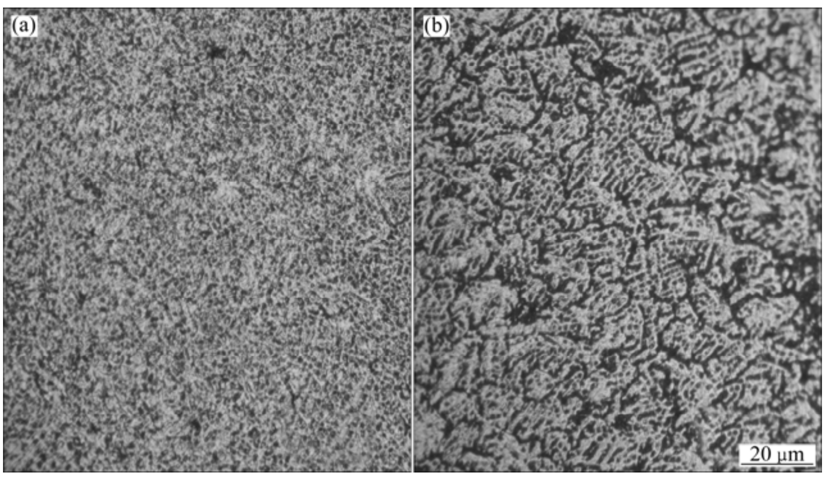

Fig.3 Microstructures of welded LF6 aluminum alloy joint: (a) Fusion zone; (b) Heat-affected zone

can be resolved from the matrix organization after corrosion, and black particles are the second phases. From Fig.3(a), it can be seen that the second phases are fine and distribute evenly in the weld zone. However, in the heat-affected zone (HAZ) (Fig.3(b)), the second phases are relatively coarse and aggregate at the grain boundaries. These impurities play a crucial role in degradation of the mechanical properties during the thermal cycling test.

3.1 Fracture characteristics and damage

The representative SEM fractographs of the welded joint specimens before and after the thermal cycling test are compared in Fig.4, which can provide rich information for the failure process.

In Fig.4(a), several particles can be seen on the fracture surface. There are no obvious voids found around these particles. However, the larger and deeper voids are observed in Fig.4(b). In the larger voids, particles are visible. The fracture of the welded joint specimens after thermal cycling mainly occurs in the HAZ. It is the evidence that voids form around the particles during the thermal cycling process. The particles in the welded joints become the source of failure under thermal cycling conditions[12−14]. The particles in the weld region were identified by means of EDS analysis. They are a complex mixture of β phase (Al_8Mg_5), impurities of Mg_2Si, and a few Al-Mn-Fe compounds.

3.2 Dislocation configuration

Dislocation configuration characteristics of samples in HAZ after 100 cycles are shown in Fig.5, in which the dark particles are believed to be the second phase particles and impurities.

As illustrated by *A* and *B* in Fig.5, the dislocation pile-up groups around the particles generate in the HAZ. Due to the large differences in thermal and mechanical parameters between these particles and the base alloy, large stresses including the mismatch stress and applied stress are induced under thermal load cycling conditions, which leads to dislocation glide. In the glide process, the blocking of the particles results in dislocation pile-up groups around these particles. The stress concentration in blocking particles owing to dislocation pile-up groups is τ:

$$\tau=n\tau_0 \tag{1}$$

where τ is the resolving shear stress value of stress concentration along the slip direction, which is caused by dislocation. According to Eq.(1), the stress concentration generated in front of dislocation pile-up groups is n times as large as τ_0. When the dislocation density around the particles accumulate to a certain degree, the stress concentration between the particles and the matrix exceeds the interface bonding strength, and micro-cracks will generate at the interface. Particles gradually separate from the base alloy with the continuation of the test cycle.

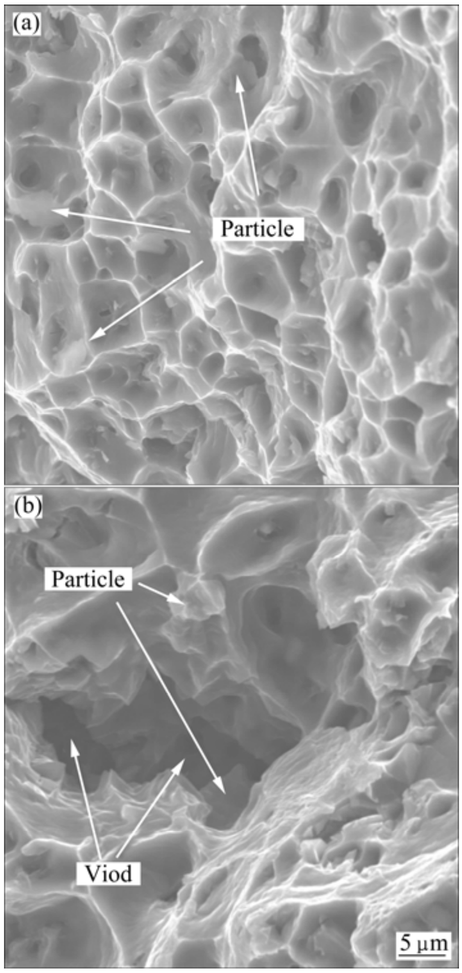

Fig.4 Representative fractographs of welded joints: (a) Before thermal cycling test; (b) After 100 cycles of thermal cycling

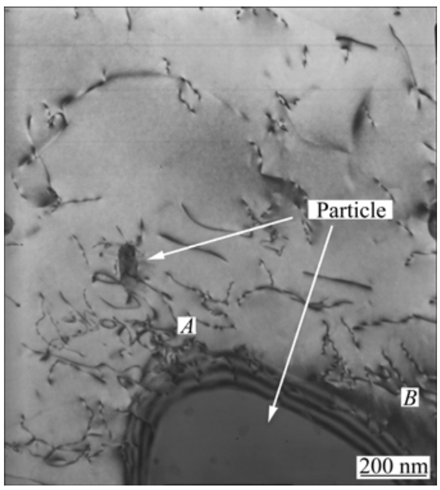

Fig.5 Dislocation configuration characteristics of samples in HAZ after 100 cycles of thermal cycling

4 Theoretical analysis of void nucleation

For the purpose of understanding the thermal cycling assisted voids formation, it is convenient to consider a spherical volume unit containing a particle of spherical shape, as shown in Fig.6[15].

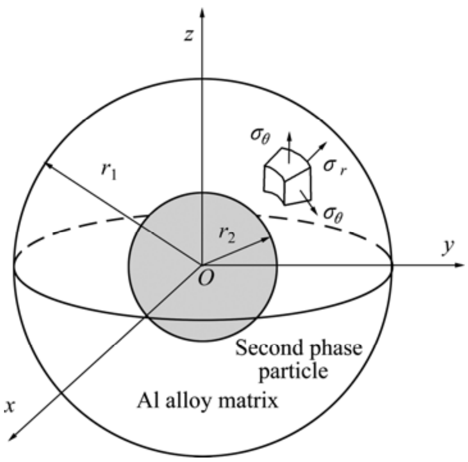

Fig.6 Spherical volume unit containing particle

Each constituent phase is assumed to be elasto-plastically perfect and isotropic solid, but the yield strength of the second phase particle is much higher than that of the Al alloy matrix. And the interface of the matrix and the second phase particle is assumed to be well bonded. From generalized Hooke's law, the strain during temperature varying can be expressed as

$$\varepsilon_r = \frac{1}{E}(\sigma_r - 2\nu\sigma_\theta) + \alpha\Delta T$$
$$\varepsilon_\theta = \frac{(1-\nu)\sigma_\theta - \nu\sigma_r}{E} + \alpha\Delta T \quad (2)$$

where E is elastic modulus, ν is the Poisson ratio, T is the temperature and α is the coefficient of thermal expansion. ε_r, σ_r and ε_θ, σ_θ are the stain, stress at radial direction and tangential direction, respectively. OLSSON et al[14] calculated the interface pressure p during temperature varying in the elasto-plastic framework with no other external load. Using subscript 1 to refer to the matrix material and subscript 2 to refer to second phase particle, the interface pressure induced by temperature varying can be expressed by[16]

$$p = \frac{\dfrac{2E_1}{3(1-\nu_1)}(\alpha_2 - \alpha_1)(1-\varphi)\Delta T}{[1 - \dfrac{2M_{\mathrm{el}}}{3}(1-\varphi)]} \quad (3)$$

where φ is the particle volume fraction, and in this unit cell, $\varphi=(r_2/r_1)^3$. M_{el} is so called elastic mismatch parameter and given by

$$M_{\mathrm{el}} = \frac{E_1}{1-\nu_1}\left(\frac{1-2\nu_1}{E_1} - \frac{1-2\nu_2}{E_2}\right) \quad (4)$$

According to Eqs.(3) and (4), we can see that the interface pressure p can be positive or negative, which indicates that the interface can be in traction during temperature varying even if there is no external stress applied. In general, $\alpha_1>\alpha_2$ and $-\infty < M_{\mathrm{el}} < 3/2$, so, when $\Delta T>0$, $p<0$, the interface is in the status of traction. This means the thermal mismatch stress p can assist the void nucleation.

Above analysis is under the condition of no external load applied. If the material is applied with an external stress during thermal cycling process, the thermal mismatch stress p can associate the external load to control the void nucleation process.

5 Numerical simulation of void nucleation

In the present study, finite element (FE) calculations of cell structures have been widely used to simulate and study the behavior of porous solids. In the numerical calculations carried out here, a cylindrical representative volume element (RVE) instead of a spherical RVE is selected because 1) the cylindrical RVE is widely used to analyze void nucleation in Gurson type porous materials[17], 2) it is convenient to apply boundary conditions and constraints, and 3) the above theoretical thermoanalysis results of the spherical RVE are very similar to the FE calculations of the cylindrical RVE as long as the particle volume fraction is not so large.

A representative cell model was established to analyze thermal stress-assisted voids formation[18]. The cell model shown in Fig.7 is assumed to be a cylinder of matrix containing a spherical particle at its center. The height of the cylinder is equal to its diameter. The radius of the particle is one fourth of that of the cylinder. Due to periodical symmetry, the cylinder can be represented by the plane $ABCD$, which can be converted into a finite element grid by using axisymmetric elements.

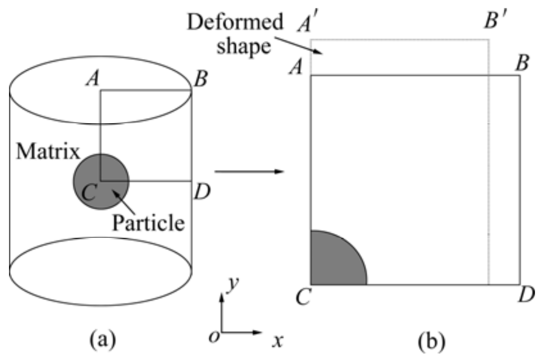

Fig.7 Cylindrical axisymmetric model: (a) Representative unit cell model; (b) Finite element cell model

The boundaries AC and CD were constrained in the y and x directions, respectively. A set of cohesive elements is modeled at the interface between the particle and the matrix. The value of debonding strain of the cohesive elements is specified as 0.1. The typical properties of the constituent phases in this unit cell model are listed in Table 3.

Two analysis steps were defined. In the first step, a constant mechanical load, $\sigma = 100$ MPa, was applied along boundary AB in the vertical direction. In the second step, a sine-type temperature cycling was superposed. The cyclic range was between 173 and 373 K and the period was 90 min.

Table 3 Typical materials parameters at 20 °C

Material	Coefficient of thermal expansion/ 10^{-6} K^{-1}	Elastic modulus/ GPa	Yield strength/ MPa
LF6 Al alloy matrix	23.86	69	157
Mg_2Si particle	7.5	120	−

The FEM simulation void nucleation in external load and thermal cycling condition is shown in Fig.8 and the stress values at the various stages of the void nucleation process were displayed by different grey scales.

As illustrated in Figs.8(a) and 8(b), it can be seen that the biggish stress can be found at the interface, and they all extend outward from the interface and reduce gradually. When the matrix and particle remain bonded, the maximum stress in the matrix does not occur at the tensile axis (A zone), but along the particle surface at

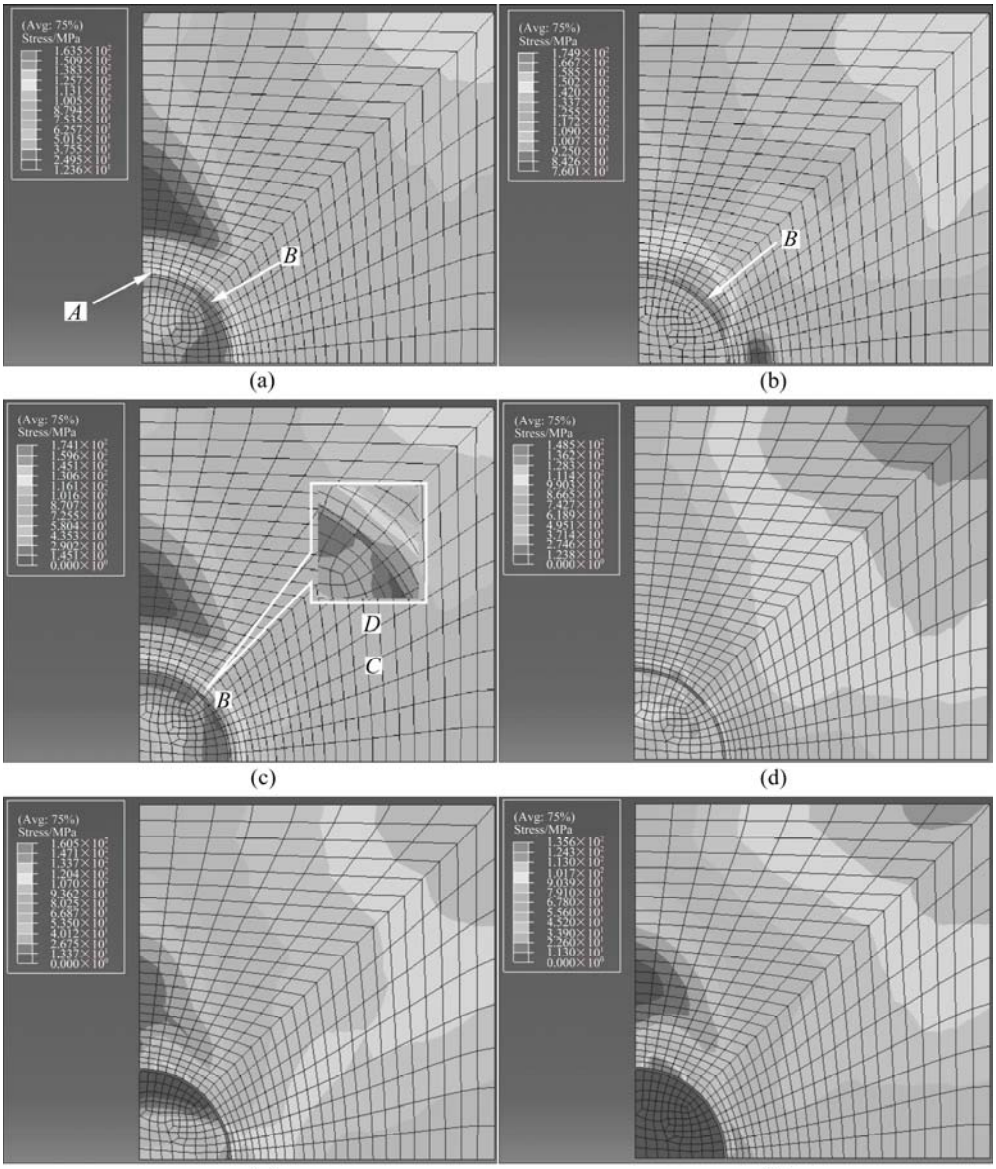

Fig.8 Simulation for void nucleation process: (a) Bonding interface; (b) Location of maximum stress; (c) First failure element; (d) Crack propagation; (e) Crack reaching tensile axis; (f) Spherical void nucleation

about 45° from the tensile axis (*B* zone). After certain times of thermal cycling in the second step, *B* zone in Fig.8(c) firstly reaches the value of debonding strain and the debonding process begins. In order to observe more clearly, *B* zone in Fig.8(c) is enlarged as shown in *D* zone. In the *D* zone, one cell at the interface at about 45° from the tensile axis has lost its efficacy. Micro-crack source firstly generates at this zone, and the crack propagates rapidly along the particle/matrix interface and then a spherical void nucleates (Figs.8(d)−(f)).

4 Conclusions

1) The VPPA welding process may introduce extra impurity particles in the HAZ of LF6 aluminium alloy welded joint. Inhomogeneity of the welded joint leads to the different fracture mechanisms during thermal cycling. The large and deep voids observed on the fracture surface for the thermally cycled samples further demonstrate the micro-void formation and evolution mechanism around the particles in the HAZ.

2) More dislocation pile-up groups form around large particles. This is the main cause for micro-cracks formation and final particle separations from the base alloy during the thermal cycling.

3) The finite element analysis of a unit cell shows that thermal cycling can cause the accumulated plastic strain at the particle/matrix interface and the nearby matrix, therefore control the process of void nucleation. Under certain conditions, the efficacy of cell at the interface at about 45° from the tensile axis disappears. Micro-crack source firstly generates at this zone, and the crack propagates rapidly along the particle/matrix interface.

References

[1] BABAEVSKY P G, KOZLOV N A, CHURILO I V. Influence of simulated and natural space environment factors on dielectric properties of epoxyamine polymers and polymer-based composite materials [J]. Cosmic Research, 2005, 43(1): 25−33.

[2] GEORGE P E, DURSCH H W. Low earth orbit effects on organic composites flown on the long duration exposure facility [J]. Advanced Materials, 1994, 25(3): 10−19.

[3] HAN J H, KIM C G. Low earth orbit space environment simulation and its effects on graphite/epoxy composites [J]. Composite Structures, 2006, 72(2): 218−226.

[4] MINGUEZ J M, VOGWELL J. Fatigue life of an aerospace aluminium alloy subjected to cold expansion and a cyclic temperature regime [J]. Engineering Failure Analysis, 2006, 13(6): 997−1004.

[5] MEI Hui, CHENG Lai-fei, ZHANG Li-tong. Damage mechanisms of C/SiC composites subjected to constant load and thermal cycling in oxidizing atmosphere [J]. Scripta Materialia, 2006, 54(2): 163−168.

[6] ZHOU Chu-wei, YANG Wei, FANG Dai-ning. Damage of short-fiber-reinforced metal matrix composites considering cooling and thermal cycling [J]. Engineering Materials and Technology, 2000, 122(2): 203−208.

[7] HEINZ A. Recent development in aluminum alloy for aerospace application [J]. Materials Science and Engineering, 2000, 280(1): 126−135.

[8] NYKANEN T, LI X, BJORK T, MARQUIS G. A parametric fracture mechanics study of welded joints with toe cracks and lack of penetration [J]. Engineering Fracture Mechanics, 2005, 72(10): 1580−1609.

[9] YAMAMOTO N, MURAI R, YOSHINARI H. Reliability based defect assessment methodology for welded joints with respected to brittle fracture [J]. Journal of the Society of Materials Science, 2007, 56(6): 544−549.

[10] WATANABE T, HONGO H, YAMAZAKI M. Mechanical properties and fracture type of dissimilar welded joint at elevated temperatures [J]. Iron and Steel Institute of Japan, 2007, 93(8): 552−557.

[11] RUBIO D, GALVEZ F, FRANCO D C, SANCHEZ V. Fracture strength of welded aluminium joints in commercial road vehicles [J]. Engineering Failure Analysis, 2006, 13(2): 260−270.

[12] TAI N H, YU H C. Effects of low-energy impact and thermal cycling loadings on fatigue behavior of the quasi-isotropic carbon epoxy composites [J]. Polymer Research, 1998, 5(3): 143−151.

[13] HAUSMANN J M, LEYENS C, KAYSSER W A. Interaction between cyclic loading and residual stresses in titanium matrix composites [J]. Materials Science, 2004, 39(2): 501−509.

[14] OLSSON M, GIANNAKOPOULOS A E, SURSSH S. Elastoplastic analysis of thermal cycling: Ceramic particles in metallic matrix [J]. Journal Mechanics Physical Solids, 1995, 43(10): 1639−1671.

[15] HAO S, BROCKS W. The Gurson-Tvergaard-Needleman model for rate and temperature-dependent materials with isotropic and kinematic hardening [J]. Computational Mechanics, 1997, 20: 34−40.

[16] NEEDLEMAN A. Computational mechanics at the mesoscale [J]. Acta Materialia, 2000, 48(1): 105−124.

[17] NIELSEN K L. Predicting failure response of spot welded joints using recent extensions to the Gurson model [J]. Computational Materials Science, 2010, 48(1): 71−82.

[18] VADILLO G, FERNANDEZ J. An analysis of Gurson model with parameters dependent on triaxiality based on unitary cells [J]. European Journal of Mechanics A: Solids, 2009, 28: 417−427.

(Edited by LI Xiang-qun)